Proceedings of the
Annual Stability Conference
Structural Stability Research Council
San Antonio, Texas, March 20-22, 2024

Buckling detection of profiled steel deck using strain measurement techniques in a new vacuum box apparatus

Hyeyoung Koh [1], Nate Opperman [2], Gowshikan Arulananthan [3], Thomas Sputo[4], Jesse C. Hampton [5], Hannah B. Blum[6]

Abstract
The structural behavior of thin-walled steel structures is complex due to their susceptibility to local buckling, which poses significant challenges in accurately measuring and analyzing their deformation shapes. Traditional strain measurement techniques such as electrical strain gauges have been utilized to evaluate structural deformations, but limitations in gauge length and quantity of gauges inhibit the ability to capture complex deformation behavior of structures. This paper proposes a novel approach that employs distributed fiber optic sensing (DFOS) to detect and analyze the deformation behavior in steel members, with a specific focus on roof deck members consisting of profiled thin-walled steel sheets. By utilizing Rayleigh Optical Frequency Domain Reflectometry (OFDR), distributed strain sensing at fine scales (e.g., mm scale gauge lengths) can be used to facilitate precise assessment of local buckling deformations.

The main objective of this study is to determine if distributed fiber optic strain sensing can be used to characterize deformation and buckling behavior of steel deck. DFOS is conducted during the experimental testing of a profiled steel deck loaded to failure inside a vacuum box chamber, which provides uniform pressure across the entire roof plane. Conventional strain gauges and an optical tracking system are also used to measure strain and deformations. The outcomes of this study contribute to an enhanced understanding of advanced measurement techniques for structural testing and introduce an innovative solution for accurate deformation detection in steel members.

1. Introduction

Steel decks are thin-walled corrugated metal sheets that can be used to support roof or flooring structures, and they are typically supported by steel beams or joists. Steel decks can be used as diaphragms to distribute wind and seismic lateral forces across a building into structural elements

[1]Postdoctoral Associate, University of Wisconsin-Madison <hyeyoung.koh@wisc.edu>
[2]Graduate Research Assistant, University of Wisconsin-Madison <nopperman@wisc.edu>
[3]Graduate Research Assistant, University of Wisconsin-Madison <arulananthan@wisc.edu>
[4]Technical Director, Steel Deck Institute <tsputo50@gmail.com>
[5]Assistant Professor, University of Wisconsin-Madison <jesse.hampton@wisc.edu>
[6]Assistant Professor and Alain H. Peyrot Fellow, University of Wisconsin-Madison <hannah.blum@wisc.edu>

that transmit them into the foundation. The thin-walled portion of decks can make them susceptible to local buckling. In conventional testing of a deck to assess its capacity, a spreader beam is used to apply load on concentrated points. A point load on thin-walled steel members could result in a localized failure. However, in a realistic setting, the deck is subjected to uniformly distributed pressure loads. Testing and analysis for steel decks under point loading has been conducted (Germund 1986, Wu et al. 1996; 1997, Bahr 2006, Vsorf and Jandera 2017, Raebel and Gwodzdz 2018; 2020), while those under distributed pressure loading are not available in the literature, which hinders the fullest understanding of steel roof deck response under load.

This project explores and validates a new test apparatus and instrumentation setup. This experimental setup can later be used to test steel deck systems to better understand their behavior and improve the reliability of steel roofing and flooring decks that are common in metal buildings. A vacuum box chamber, which produces uniform pressure loading by creating a negative pressure inside the box by removing air out of the box, was fabricated to simulate distributed gravity load. When air is pulled out from the box, uniform pressure is applied across the deck surface. Two nested 3-foot (0.9 m) $\times$ 16-foot (4.9 m) steel decks were tested. To detect local deformation of the deck specimens, novel sensing techniques including fiber optic sensing and an optical tracking system were employed. The outcome of this study will (1) validate the new experimental setup, (2) demonstrate the capabilities of novel sensing techniques in structural testing, and (3) enable future testing towards the Holistic Steel Systems effort https://ssirl.cee.wisc.edu/holistic-steel-systems/.

2. Experimental study

2.1 Vacuum box

To test how steel deck roofing systems perform under realistic loading conditions, an 8-foot (2.4 m) by 16-foot (4.9 m) box, standing about 3 feet (0.9 m) tall, was constructed using wood panels (Figure 1). The box was bolted to the floor to maintain structural integrity during tests. Designed with modular 4-foot (1.2 m) sections, it can be adjusted in size as needed for future tests. A steel deck can be placed across the top, and during tests, vacuums are used to siphon air out of the inside of the box to create pressure loads. Three valves including the Gate valve, the Motorized valve, and the Red valve, as shown in Figure 2, control pressure throughout the box during tests. A pressure transducer measures pressure inside the box. Several flanges are installed on the side of the box to bring cables from instrumentation inside the box to the exterior. A plastic tarp covers the top of the box and is sealed with double-sided tape along the top edges to seal the chamber. Derived from the operation of valves and vacuums used to pull out air out of the box, this experimental apparatus was named the SEAhorse (Suction Experimental Apparatus).

Two 3-foot (0.9 m) by 16-foot (4.9 m) decks were nested along the longitudinal edge, therefore a plane profile of the specimen is 6-foot (1.8 m) wide and 16-foot (4.9 m) long. Figure 3 shows the deck cross-section profile, which has a depth of 1.5-inch (38 mm), a flat region on top flange of 3.2-inch (81 mm), a flat region on the bottom flange of 1.3-inch (33 mm), and a corner radius of 0.2-inch (5 mm). A 22 gauge wide rib roof deck, 0.03-inch (0.76 mm) thick, was tested (1.5WR22). The decks are simply supported at the center and 8 inches (203 mm) in from the deck edges. Screws were used to attach the bottom flanges of the deck profile to the supports. Figure 2 provides a photo of the deck installed on the vacuum box. A 2-foot wide strip of plywood was placed next to the 6-foot wide deck to fill the remaining space to the box edge.

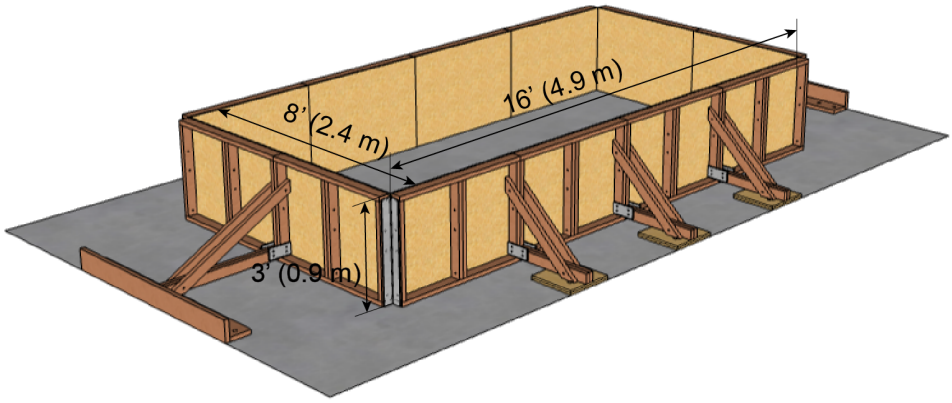

Figure 1: 3-dimensional model of the vacuum box without a deck specimen

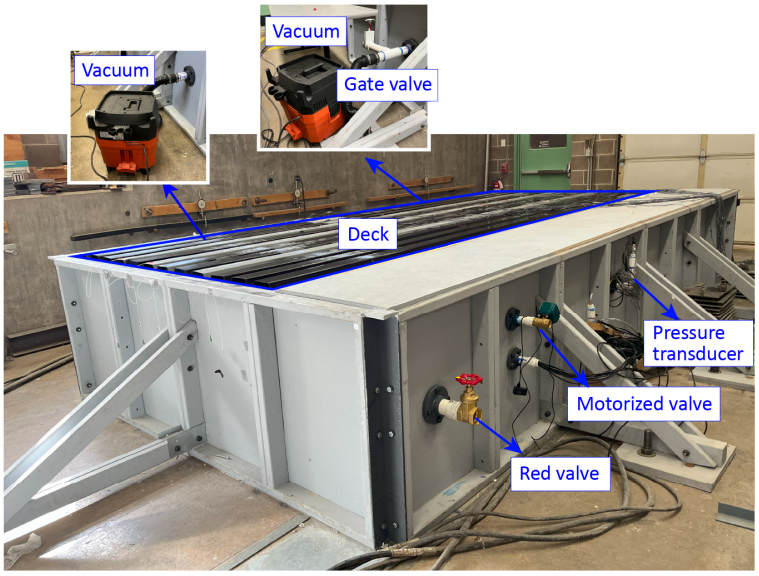

Figure 2: The vacuum box, SEAhorse

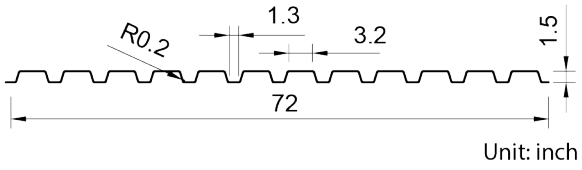

Figure 3: 1.5WR22 deck profile

The deck specimens had a nominal yield strength of 80 ksi (550 MPa) and an nominal elastic modulus of 29,500 ksi (203 GPa). Due to lab renovations, the equipment for tensile coupon tests was not available prior to submission of this paper.

2.2 Test procedure

Three valves and two vacuums were employed to apply pressure load to the decks. Figure 2 shows the locations of the valves and the vacuums on the box. Step-by-step instructions for removing air inside the box are provided below. To ensure a consistently increasing pressure load, the number and degree of valve turns were determined based on preliminary testing results that measured the pressure load versus the degree of valve turns.

1. Start with all the three valves open.
2. Turn on the two vacuums.
3. Close the Gate valve at the vacuum, initiating the pressure load to approximately 10 psf (479 Pa).
4. Begin closing the Red valve while monitoring pressure changes.
   (a) For the first four complete turns, the pressure rise should be minimal, up to about 20 psf (958 Pa). Turn the valve a half ($\frac{1}{2}$) turn when the pressure stabilizes.
   (b) After the fourth turn through the sixth turn, a half turn should take about 30 seconds.
   (c) After the sixth turn through valve being completely closed, a half turn of the valve should take about 60 seconds.
5. Begin closing the Motorized valve. The Motorized valve closes slowly—Close the valve by 10 percent no more frequently than every 30 seconds.
6. Complete the test: Once the desired pressure is achieved and the test is completed, open the Gate valve to release the pressure, and turn off the vacuums. In this study, a maximum desired pressure of 100 psf (4.8 kPa) was considered.

3. Instrumentation

To measure the local deformation of the decks under uniform pressure load, this study employed fiber optic sensing and conventional electric strain gauges for strain and an optical tracking camera system for displacement.

3.1 Fiber optic sensing

Within the last decade, DFOS has increasingly become prevalent in structural health monitoring (SHM) applications to obtain strain and temperature measurements from civil engineering structures of interest. DFOS systems enable spatially continuous measurements of strain and temperature to be made along a length of fiber. This provides an advantage over traditional strain gauges and Fiber Bragg Grating (FBG) sensors which only provide discrete measurements. DFOS systems

exploit inhomogeneities inside the fiber optic cables to measure subtle changes along the length of the fiber from both mechanical- and temperature-induced strains (Lu et al. 2019). Changes in the external environment will affect the position of the inhomogeneities along the cable. The change in position is then converted to a strain value. An interrogator sends laser light through the fiber, which interacts with the defects inside the fiber. Some of this light is reflected to the interrogator unit as backscattered light at specific frequencies.

Three different scattering mechanisms are utilized to gather strain and temperature information, e.g., Raman, Rayleigh, and Brillouin scattering. The fiber optic sensing method used to analyze strain in the steel deck is Rayleigh OFDR. Rayleigh OFDR uses a swept-frequency laser pulse to generate an interference pattern from the backscattered light which is analyzed to return location and strain information along a fiber optic cable (Liang et al. 2021). Rayleigh OFDR has been deployed to monitor strains in concrete and steel structures with high accuracy. Sensors installed in reinforced concrete buildings have been demonstrated to locate cracks in concrete (Brault et al. 2019) and monitor deformation and damage in model steel bridges (Van Der Kooi and Hoult 2018).

The ODiSI 6100 Rayleigh OFDR system by LUNA Innovations was used in this experimental study to capture longitudinal strain along the steel deck. The gauge length used in this experiment was 2.6mm with a sampling rate of 6.25 Hz. The gauge length of a DFOS system is the shortest distance over which a strain or temperature measurement could be obtained.

Fiber optic cables were attached to measure longitudinal strains on the top surface of the deck. Figure 4(a) illustrates the layout of the fiber optic cables. Four flange locations, including two bottom flanges (FLB1 and FLB2) and two top flanges (FLT1 and FLT2), were selected. The instrumentation naming convention is provided in Figure 5. To prepare the deck surface for fiber cable installation, the deck surface was cleaned using acetone. The fiber cables were then glued using M-Bond 200, manufactured by Vishay Measurements, across the deck span.

Strain gauges were installed as close as possible to the fiber optic cables at specific locations to cross-check the strain values obtained from fiber optic cables. Strain gauges, FLA-5-11-3LJCT, manufactured by Tokyo Measuring Instruments Laboratory, were employed. Thirteen longitudinal strain gauge locations (SLB1 through SLB5 and SLT1 through SLT8) were determined based on the significant locations of the deck span behaviors. For instance, SLB1, SLT1, and SLB4 are positioned at the middle support; SLB2, SLT3, SLB5, SLT5, and SLT8 are located at the midpoint between the center support and the end support; SLB3, SLT4, and SLT6 are at the end support; SLT2 and SLT7 are positioned 14 inches (35.6 cm) away from the center support, which can show strain variations between the center support and the middle span. Additionally, strain gauges measured strains in the transverse direction (STT1, STT2, and STT3) at the third point of the middle span between the end supports. Figure 6 shows the installed strain gauges alongside the fiber optic cables in the longitudinal direction.

3.2 Optical Tracking System

Optical tracking is a method of determining in the real-time position of an object by tracking the positions of markers attached to it. The position of the reflective point is determined using a camera system. In this study, to capture the motion of the deformed deck subjected to increasing

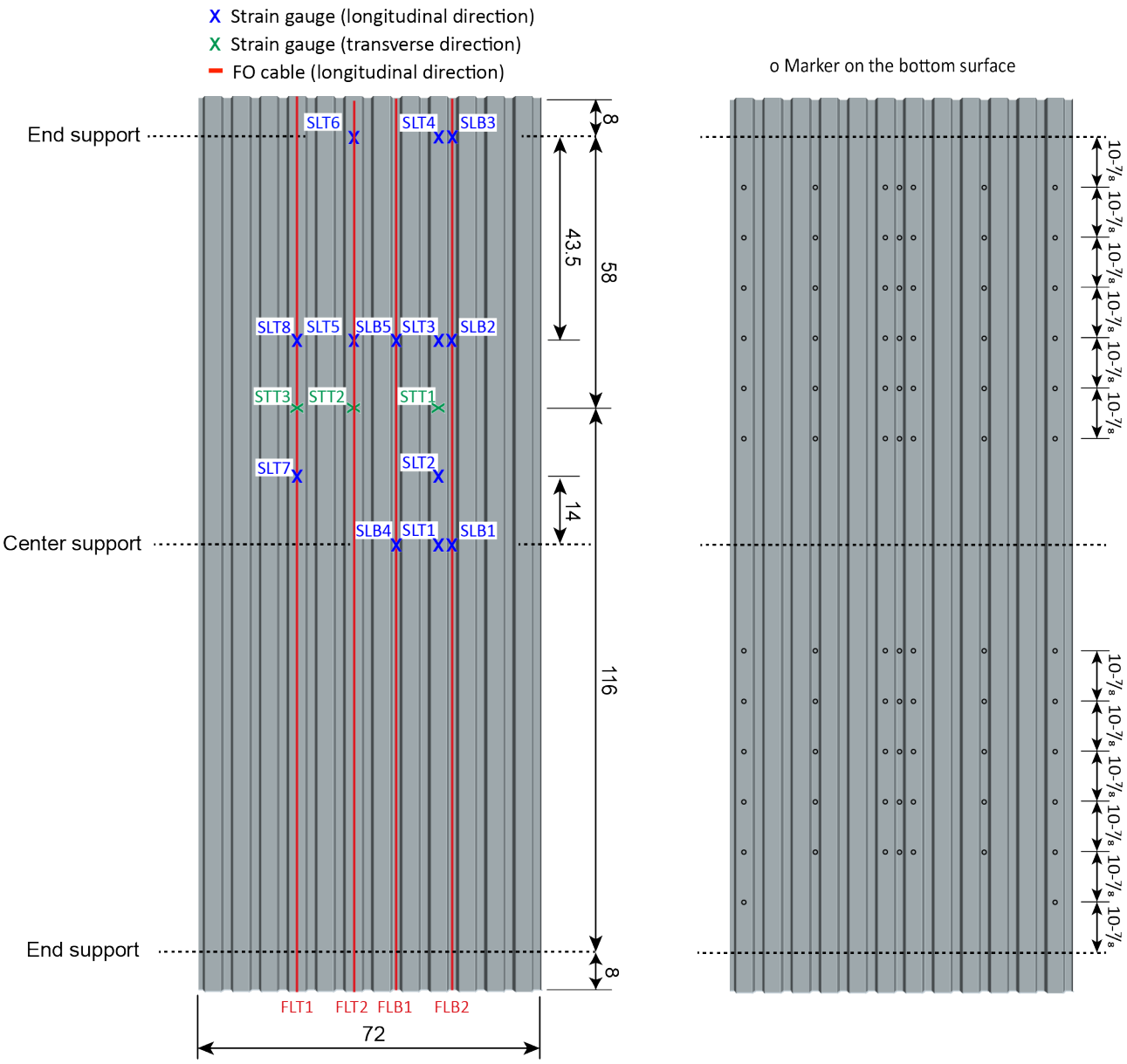

Figure 4: Diagrams of the fiber cable and strain gauge locations (left) and marker positions (right). Unit: inch.

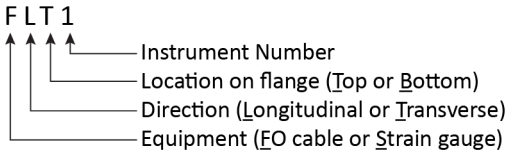

Figure 5: Instrumentation tags

Figure 6: Fiber optic cables and strain gauges at SLB1 and SLT1

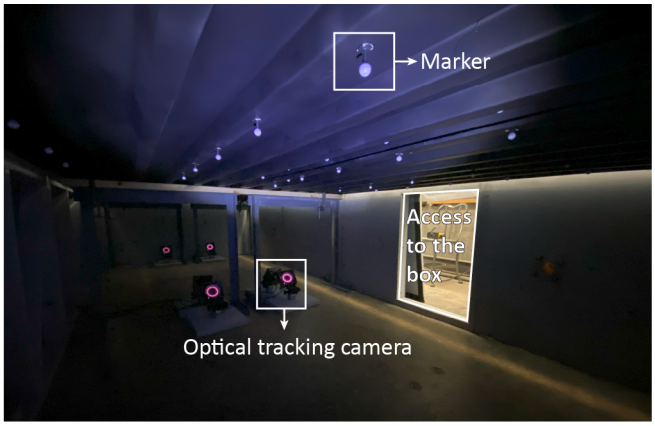

Figure 7: Optical tracking cameras and markers installed on the underside of the deck

pressure load, the Optitrack motion capture system was employed with an overall accuracy of 0.1 mm (0.004 in.). Markers were installed on the underside of the deck specimen to avoid conflicts with fiber optic cables and strain gauges on the upper surface. As the steel deck surface is shiny and reflective, it was necessary to paint the deck underside matte black to reduce light reflections. The cameras use infrared to track the positions of the markers, and reflections from the shiny deck created interference. The deck painting created an extra step in specimen preparation but was necessary to ensure the accuracy of the optical tracking system. Figure 4(b) illustrates the marker positions. Seventy-nine markers were attached to the underside of four top flanges and three bottom flanges. The markers were positioned along the deck spans between the end and middle supports. Due to the presence of supports underneath the deck specimen, markers were not able to be placed in those support positions. As shown in Figure 7, the markers were affixed to the bottom surface of the deck specimen, with optical tracking cameras positioned on the floor inside the box. Eight cameras were used to capture deformations, with four cameras directed towards each half of the deck.

4. Results

Pressure loading was applied following the test procedure introduced in Section 2.2. As shown in Figure 9(a), closing the Gate valve at the beginning increased the pressure rate up to 13 psf (0.6

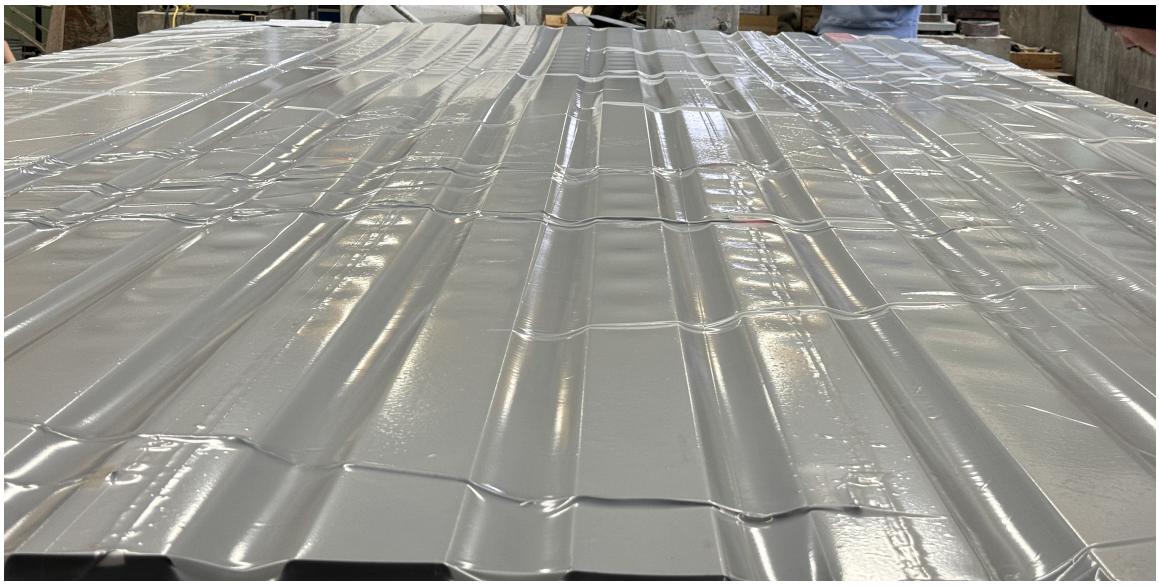

Figure 8: Deformed deck during test showing local buckling in top flange

kPa). Subsequently, the pressure rate increased to approximately 70 psf by closing the Red valve. The valve rotation was then paused for about 800 seconds to assess local buckling on the top flange of the deck. The test was completed once the pressure neared the target pressure of 100 psf. A photo of the deformed deck during testing is shown in Figure 8. The gates were then opened and vacuums turned off, at which time the deck returned to the initial position. No evidence of plastic deformation was visible.

4.1 Strain

Figure 9(b) provides the strain results measured at SLT5 and SLT6 on the top flange. SLT5 is positioned at the midpoint between the center support and the end support. The strain at SLT5 initially shows increasing compressive strain until the pressure reaches 40 psf (1.9 kPa), after which it decreases. This may be due to the position of the strain gauge relative to the local buckling waves. At approximately 60 psf (2.9 kPa), SLT5 shows tensile strain. SLT6 is positioned at the end support, where it shows a minimal strain compared to other locations along the deck span. As SLT6 is positioned at the top flange, the strain value at maximum pressure shows a positive strain.

Figure 9(c) shows the strain results at SLB1, SLB2, and SLB3 on the bottom flange. SLB1 at the center support exhibits compressive strain throughout the pressure range. SLB2, positioned at the midpoint between the center support and the end support, shows tensile strain. The strain magnitude at SLB1 is shown to be greater that at SLB2. Similar to SLT6 shown in Figure 9(b), SLB3 at the end support shows minimal strain, which is compressive, contrasting with the strain at SLT6. This difference arises because SLB3 is positioned at the bottom flange.

Strain transverse to the deck span was measured using strain gauges. Measurements were taken at three positions on the top flange: STT1, STT2, and STT3, with the third point located between the end supports. Figure 10 shows the strain values versus pressure loads. As expected, these strain values were minimal compared to the longitudinal strain results shown in Figures 9(b) and (c),

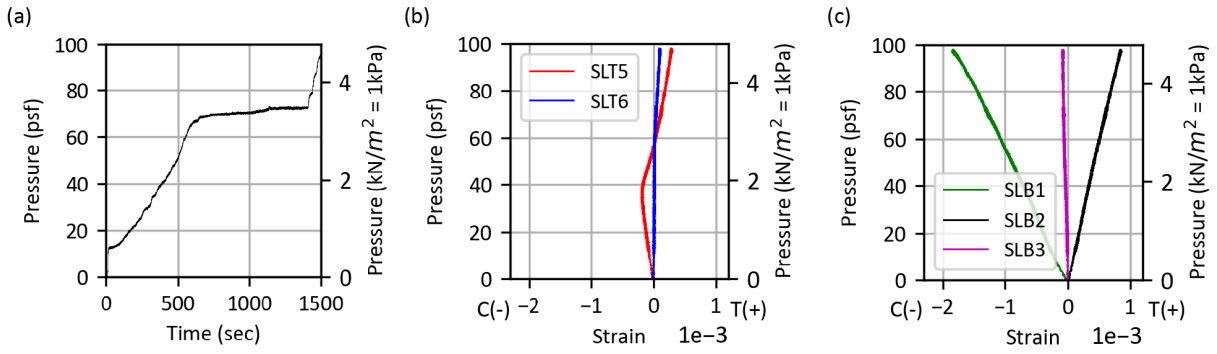

Figure 9: (a) Pressure rate (b) Longitudinal strain results at SLT5 and SLT6 (c) Longitudinal strain results at SLB1 through SLB3

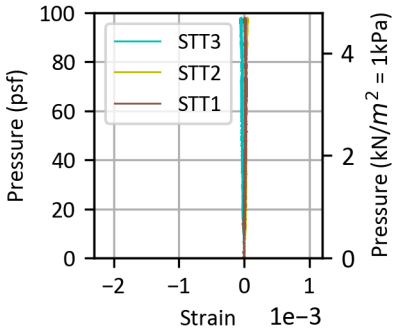

Figure 10: Transverse strain results

measuring only 1.00e-3 under the maximum pressure.

Initial interpretations of the test results show that the Rayleigh OFDR system could identify multi-scale strains, including the global deformation of the deck as well as local buckling of the deck top flanges. Figure 11 provides the strain distributions, obtained from the Rayleigh OFDR system, of the four flanges (FLT1, FLT2, FLB1, and FLB2) illustrated in Figure 4. The position along fiber (x-axis) represents the deck flange span. The strain distributions were captured at two pressure rates: 21 psf (1.0 kPa) and 97 psf (4.6 kPa), respectively. The distributions of the bottom flanges (FLB1 and FLB2) show global buckling, represented by a significant wave along the fiber length. However, the top flanges (FLT1 and FLT2) present smaller wave shapes within the larger wave across the fiber length. The small wavelength indicates local buckling occurred on the top flanges. As expected, the magnitudes of local buckling waves are larger at the middle span between the end and center supports. Unlike discrete strain measurement obtained from strain gauges, the fiber optic sensing approach demonstrated its capability for distributed sensing which enables the capture of local and global behaviors of steel members.

Figure 12 shows the time-varying strain distributions of FLT1. At 1650 seconds, the pressure rate reached 97 psf (4.6 kPa), which is the maximum considered in this study. The color bar on the right represents strain magnitudes, with red indicating tension and blue indicating compression. As

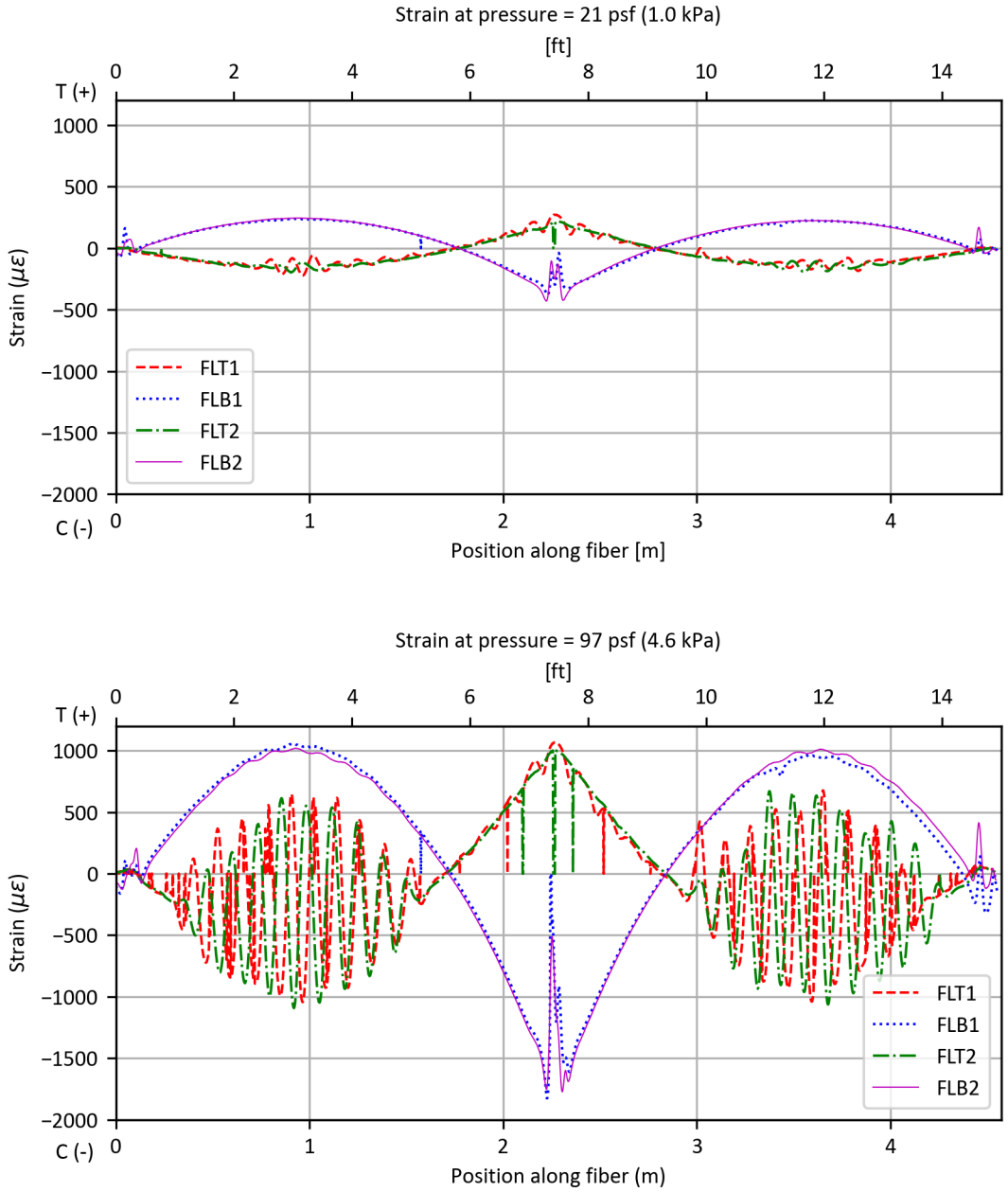

Figure 11: Strain distributions obtained from the Rayleigh OFDR system. Top plot shows measured strain along each fiber at 21 psf where initiation of local buckling (high frequency variations) can be observed. Bottom plot shows strains at 97 psf on top and bottom flanges.

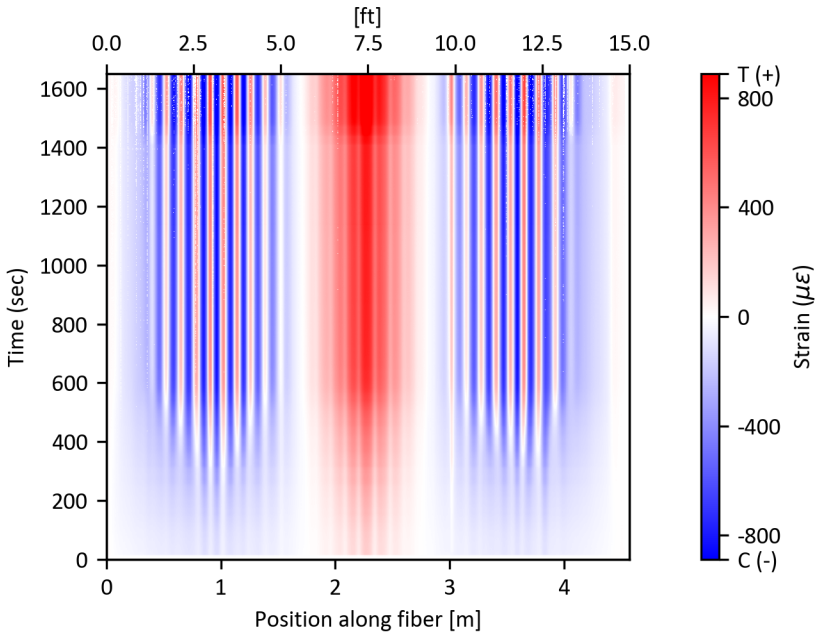

Figure 12: Strain distributions of FLT1 varying over time. Refer to Figure 4 for the location of FLT1 on the steel deck.

expected, the strain magnitudes increase with time since the pressure is increased with time. The position along fiber (x-axis) represents the deck flange (FLT1) span. Tension strain occurred near the center support, and waves of tension and compression are observed between the end support and center support, representing local buckling on FLT1. This demonstrates that the fiber optic sensing approach can detect local buckling deformations and measure the magnitude change over time.

4.2 Deformation

Figure 8 provides the 3-dimensional deformation of the deck as captured by the optical tracking camera system. The black lines represent the reference line of the marker borders, while a blue line denotes the reference line of one of the top flanges, FLT2. In Figure 13(b), the deformation of FLT2 is shown from an approximate elevation view, presenting a different angle of viewport compared to the illustration of the entire markers in Figure 13(a). The optical tracking results indicate that the FLT2 deformation, defined as the distance between the undeformed and deformed marker positions, is larger for the markers located at the mid-span between the center support and end support in comparison to those closer to the supports. This demonstrates that the optical tracking camera system can be utilized to assess the spatial deformation of structures.

5. Discussion

When the pressure loading reached approximately 60 psf (2.9 kPa), local buckling occurred on the top flanges, as shown in Figure 8. This phenomenon was observed between the center support

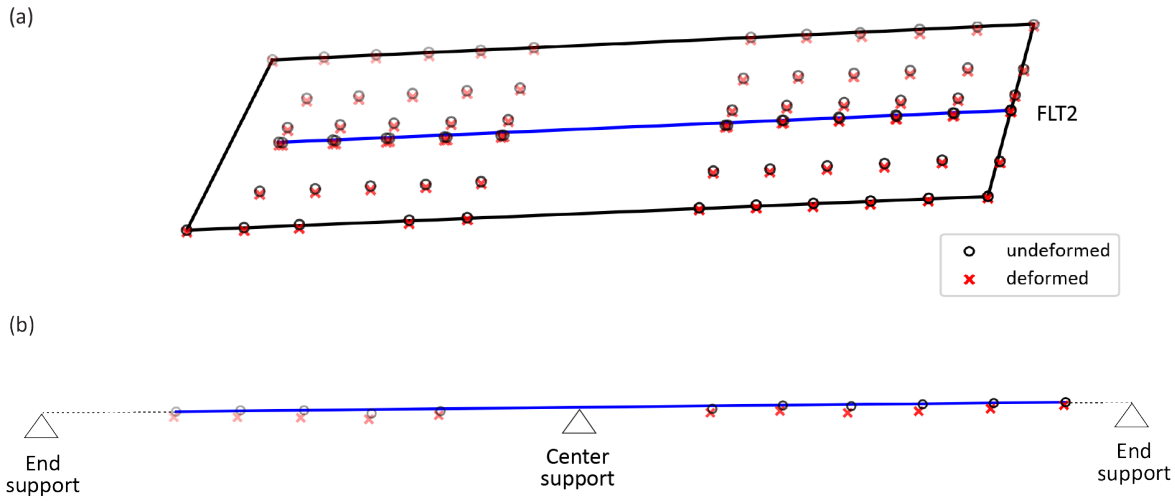

Figure 13: Deformation measured by the optical tracking camera system

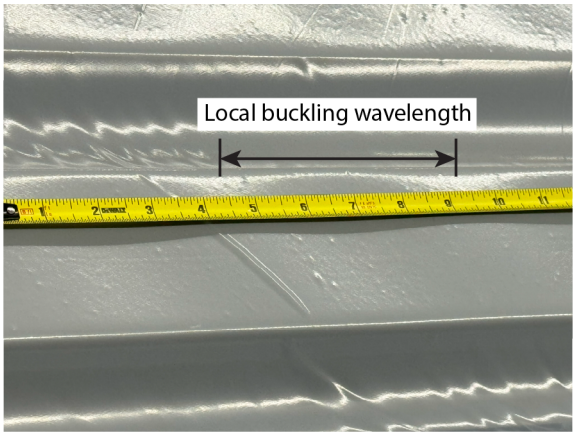

Figure 14: Local buckling wavelength

and the end support, with a local buckling wavelength of approximately 4.75 inches (121 mm) as shown in Figure 14. This observation indicates that the developed vacuum box can effectively load the deck in uniform pressure and the test setup does not suffer from issues of localized buckling due to conventional spreader beams.

In addition to demonstrating the capabilities of SEAhorse, this test investigated the potential of using fiber optic sensing to detect local buckling modes and overall deck deformation. It was also determined how to use the optical tracking system inside the vacuum box on a reflective metal surface. Overall, the three types of instrumentation worked well together and validated the overall testing method.

5.1 Future Work

This test validates the operation and control of the vacuum box to produce pressure loading for steel deck testing. It also demonstrates the capabilities of fiber optic sensing to detect global and local buckling of the steel deck. The next step is to calibrate the fiber optic cables via instrumented

tensile coupon tests, where multiscale strains can be captured by DFOS, foil strain gauges, and digital image correlation.

Additional deck tests will be conducted with different span sizes or/and deck type to force additional buckling modes. The decks will also be tested to induce plastic deformations and to overall destruction. This will enable further comparisons between the output from the fiber optic cables and conventional strain measurements when plastic buckling deformations are involved.

6. Conclusions

This study constructed a vacuum box chamber, named the SEAhorse (Suction Experimental Apparatus), to evaluate the behavior of corrugated steel decks under uniform pressure loads. The loading simulation is accomplished by extracting air from the chamber, which suctions the deck downward and simulates a uniform pressure load across its entire surface. This testing approach provides more realistic data regarding how a steel deck might perform in real-world circumstances, thereby enhancing the reliability of deck and deck systems testing. To measure distributed strain over the deck span, a distributed fiber optic sensing technique was employed along with electric strain gauges at several locations. Distributed fiber optic strain captured both the overall global deformations of the deck in addition to local buckling deformations along the top flanges. Three-dimensional deformations were captured by the optical tracking camera system located inside the box. This pilot study shows how modern instrumentation can be combined to create a comprehensive experimental system to measure detailed strain, buckling, and deformations.

Acknowledgement

The vacuum box portion of this project was funded by the Steel Deck Institute, with material donations from Canam Steel Corporation, DACS, Inc., Gooder-Henrichsen Co., New Millennium, Nucor Corporation, and Simpson Strong-Tie. The fiber optic sensing portion of this project was supported by a cooperative agreement with the U.S. Army Engineer Research and Development Center's (ERDC) Construction Engineering Research Laboratory (CERL).

References

Bahr, Eric Stephen (2006). *Transverse load distribution for a concentrated load on steel deck with plywood overlay*. Tech. rep. University of Missouri–Rolla.

Brault, Andre et al. (2019). "Monitoring of beams in an RC building during a load test using distributed sensors". *Journal of Performance of Constructed Facilities* 33.1, p. 04018096.

Germund, Johansson (1986). "Single load on trapezoidal steel sheet". Vol. 49. Reports of the Working Commissions (International Association for Bridge and Structural Engineerin, pp. 99–106.

Liang, Changshuo et al. (2021). "A comprehensive study of optical frequency domain reflectometry". *IEEE Access* 9, pp. 41647–41668.

Lu, Ping et al. (2019). "Distributed optical fiber sensing: Review and perspective". *Applied Physics Reviews* 6.4.

Raebel, Christopher H and Dawid Gwodzdz (2018). *Comparison of experimental and numerical results for flexural capacity of light-gage steel roof deck*. Tech. rep. Missouri University of Science and Technology.

Raebel, Christopher H and Dawid Gwozdz (2020). *Experimental and Numerical Comparison of Flexural Capacity of Light Gage Cold Formed Steel Roof Deck*. Tech. rep. American Iron and Steel Institute (AISI).

Šorf, Marek and Michal Jandera (2017). "07.09: Trapezoidal sheet hangers and concentrated or linear load distribution in profiled sheeting". *ce/papers* 1.2-3, pp. 1563–1570.

Van Der Kooi, Kyle and Neil A Hoult (2018). "Assessment of a steel model truss using distributed fibre optic strain sensing". *Engineering Structures* 171, pp. 557–568.

Wu, Shaojie, Wei-wen Yu, and Roger A LaBoube (1996). *Flexural strength of cold-formed steel panels using structural grade 80 of A653 steel*. Tech. rep. University of Missouri–Rolla.

Wu, Shaojie, Wei-wen Yu, and Roger A LaBoube (1997). *Strength of flexural members using structural grade 80 of A653 steel (web crippling tests)*. Tech. rep. Missouri University of Science and Technology.